

Adaptive Compliance Shaping with Human Impedance Estimation

Huang Huang¹, Henry F. Cappel², Gray C. Thomas^{1,3}, Bingham He¹ and Luis Sentis²

Abstract—Human impedance parameters play an integral role in the dynamics of strength amplification exoskeletons. Many methods are used to estimate the stiffness of human muscles, but few are used to improve the performance of strength amplification controllers for these devices. We propose a compliance shaping amplification controller incorporating an accurate online human stiffness estimation from surface electromyography (sEMG) sensors and stretch sensors connected to the forearm and upper arm of the human. These sensor values along with exoskeleton position and velocity are used to train a random forest regression model that accurately predicts a person’s stiffness despite varying movement, relaxation, and muscle co-contraction. Our model’s accuracy is verified using experimental test data and the model is implemented into the compliance shaping controller. Ultimately we show that the online estimation of stiffness can improve the bandwidth and amplification of the controller while remaining robustly stable.

I. INTRODUCTION

Robotic exoskeletons have been used for a range of applications including assistance with muscle impairment due to disease [1], [2], [3], control mechanisms for tele-operational robots [4], [5], and a means to augment the strength or increase the endurance of the human operator [6], [7], [8], [9]. Some researchers improve the performance of exoskeletons through feedback control [1] or offline and online optimization of control parameters [8], [10]. This paper aims to improve the performance of a force amplification exoskeleton using adaptive compliance shaping.

Force amplification exoskeletons, like impedance controlled robots for physical human robot interaction, need to maintain coupled stability with humans. Medically oriented studies often model the human as a spring, mass, damper system that dynamically changes properties as the person moves her or his joint [11], [12]. In human robot interaction to ensure stability despite uncertainty the human is often robustly modelled [13], frequently as a passive system [6], [14]. However, modelling the human as a passive system has proven to be too conservative in human robot interaction [15]. On the contrary accurate estimation of human impedance parameters have the capability to significantly improve the performance of human robot interaction [6], [13], [16].

For amplification exoskeletons, various control strategies have amplified the strength of the human by a significant factor using adaptive control [17], admittance control [18]

and impedance control [19]. Some controllers rely on robust models of the human to guarantee stability [6], [7]. Methods used include a controller using bounded uncertain human impedance [7] and a compliance shaping controller [6]. Ref. [7] maximized amplification while remaining robustly stable and used system identification with the human in the loop in order to obtain a robust model. However, the performance of this controller was limited by the amount of uncertainty in the model. The researchers in [6] tried to remove this uncertainty by inserting a physical spring between the human and the robot. The spring stiffness was known and provided a minimum compliance for the spring and human system, reducing uncertainty. However, an online estimation of human stiffness could take the place of the physical spring and increase the bandwidth of the controller.

A common approach to calculate human stiffness involves imposing a perturbation torque first proposed by [20] to calculate hand stiffness in isometric conditions. However, this method is only effective offline [21], [22], [23]. Some studies have estimated stiffness online outside of implementation into an amplification controller. These methods include biological models [23], [24], [25] as well as artificial neural networks [21], [22]. Some models hold the advantage of being able to be generalized to multiple subjects [23], [25]. Most studies focusing on stiffness estimation use sEMG sensors [21], [22], [23], [24], [25], but different sensors may provide a less noisy means to gain information from the human [26]. An optimal approach may be a combination of sEMG sensors with a secondary sensor, which is the method we use in this paper. Although many studies have successfully estimated human impedance parameters, to our knowledge no previous work has explored combining multi-modal human impedance online estimation with an exoskeleton compliance shaping strength amplification controller, which is the focus of this paper.

Research has been done to incorporate estimation of human properties to improve performance of controllers [27], [28], [29], but most studies focus on the estimation of applied torque or human intention [19], [30], [31], [32]. In many cases this torque estimation can be replaced with the measurement of the contact force between the human and exoskeleton and has limited applications for strength amplification exoskeletons (which normally contain these sensors). The researchers in [29] perform a dynamic stiffness estimation using a musculoskeletal model for a power assist exoskeleton, but focus on the reduction of vibration instead of amplification. There is still a gap in literature between online estimation of human impedance, specifically human muscle stiffness, and use in strength amplification exoskele-

The authors are with the ¹Department of Mechanical Engineering and ²Department of Aerospace Engineering in the University of Texas at Austin

³The author is supported by a NASA Space Technology Research Fellowship (NSTRF) NNX15AQ33H.

Send correspondence to huangh at utexas dot edu.

tons.

This paper proposes an adaptive compliance shaping controller using online stiffness estimation. The contributions are twofold. First, we demonstrate an accurate online estimation of stiffness using a random forest regression model and a dual biological sensor approach using stretch and sEMG sensors. Second, we validate the performance improvement of a compliance shaping controller incorporating this online estimation by increasing both bandwidth and stability.

II. ONLINE STIFFNESS ESTIMATION

We first propose an approach to estimate human stiffness online by using a trained random forest model taking advantage of data from sEMG and stretch sensors as well as exoskeleton velocity and position.

A. Apparatus

We use a single degree of freedom elbow joint exoskeleton for this research. The P0 exoskeleton from Appttronik Systems, as shown in Fig. 1, is a 3 bar linkage device powered by a series elastic actuator (SEA) with a spring force tracking bandwidth of 10 Hz and reliable actuator torque conversion using a linkage table. The exoskeleton includes a 6-axis force torque sensor measuring the human exoskeleton contact forces. The human rests his or her upper arm on a white 3D printed mount beside the actuator. Exoskeleton position θ is measured by an encoder at the joint and contact torque τ_c is measured by the force torque sensor. The moment of inertia of the exoskeleton is $0.1 \text{ kg} \cdot \text{m}^2$ without any additional weight, but provides the option to include additional external weights. A laser pointer is attached to the end of the long bar to assist with precise position movement projecting onto a white board one meter in front of the subject wearing the exoskeleton. The white board contains three lines referring to initial position and upper and lower bounds of movement. A deviation around $\pm 3^\circ$ from those lines is acceptable.

In addition, we utilize 3 Myowear sEMG sensors located on the upper arm and forearm (biceps brachii, triceps brachii, and brachioradialis muscles) of the subject and 2 Images Scientific 6" and 8" stretch sensors attached around the middle of the forearm and upper arm connected to an Arduino Mega 2560 by a breadboard. The sampling frequency for all sensors is 250 Hz. The full setup of the apparatus including the exoskeleton and the peripheral sensors are shown in Fig. 1.

B. Experimental Protocol

The experimental protocol was approved by the Institutional Review Board (IRB) at the University of Texas at Austin. The participant wears 3 sEMG sensors and 2 stretch sensors during the experiments.

The experiments are divided into 2 sections. The first consists of the participant maintaining a constant equilibrium position while the exoskeleton imposes a bias force and a sinusoidal torque with constant frequency and amplitude. In order to obtain reference values for all sensors the participant initially holds a constant posture for 20 seconds

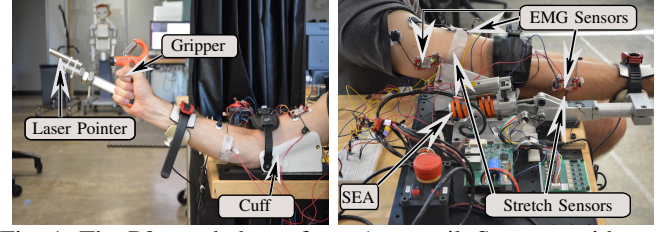


Fig. 1: The P0 exoskeleton from Appttronik Systems with an ATI Mini40 force sensitive cuff and a P170 Orion air cooled series elastic actuator. The setup includes 3 Myowear sEMG sensors and 2 Images Scientific stretch sensors connected to the human.

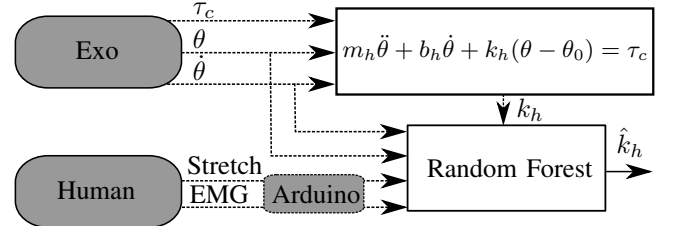


Fig. 2: Diagram of training scheme for random forest predictor.

indicated by the laser pointer pointing to the middle line on the whiteboard. The first 20 seconds includes gravity compensation without a bias force. Following this procedure the exoskeleton induces bias forces ranging from 0 Nm to 9.5 Nm in 0.5 Nm steps occurring in 3 second intervals. The participant is asked to maintain the same constant position and apply no voluntary force. The movement then is caused only by a sinusoidal signal with a constant frequency of 1 Hz and amplitude of 1.5 Nm. There is no gripper used in the first experiment, but for the purpose of inducing muscle co-contraction the participant squeezes a gripper beginning with 22 lb for the second experiment and up to 82 lb for the final experiment. There are a total of 11 experiments for this section with a 30 second resting period between each bias force transition as well as a minimum of 2 minute resting period between each experiment. This set of experiments is denoted as I.1-11.

The second set of experiments maintains the same procedure as the first experiment set except the participant voluntarily moves his or her arm at 0.5 Hz producing an oscillation about the middle line position with a range bounded between the lower and upper line of the whiteboard. Additionally, we impose a 1.7 Hz sinusoidal perturbation with an amplitude of 2.5 Nm. The bias force increases from 0 Nm to 8 Nm in step of 2 Nm occurring in 15 second intervals. All other parameters and procedures remain consistent with the first set of experiments. This set of experiments is denoted as II.1-11.

C. Methods

1) *Data Preprocessing*: In both experiment sections data from 3 sEMG sensors is amplified, rectified, and integrated and then passed through a second order low pass filter with

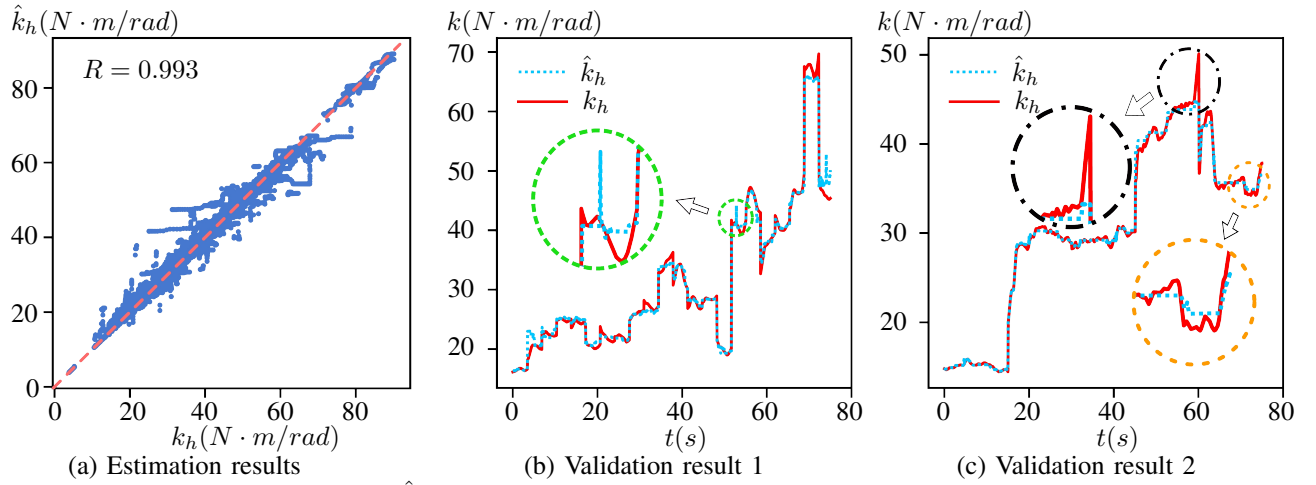


Fig. 3: Random forest predictor results. \hat{k}_h is the estimated stiffness from our random forest predictor and k_h is the reference stiffness calculated from the time domain regression. Fig. 3(a) shows the linear relationship between the estimated stiffness and the reference stiffness for all experiments I.1-11 and II.1-11. The blue dots are the data points and the red dash line is the reference line of $y = x$. Fig. 3(b) shows validation results from experiment group I. Fig. 3(c) shows validation results from experiment group II.

cutoff frequency of 60 rad/s and damping ratio of 0.707. We use the average values from 2 stretch sensors and 3 sEMG sensors in the first 20 seconds of each experiment as initial reference values for that experiment. These values are subtracted from the sEMG and stretch sensors' data to get the variation data for the 5 sensors. The absolute values of processed data from the stretch and sEMG sensors are denoted as $S1$, $S2$ and $E1$, $E2$, $E3$ respectively.

In the first experiment section, exoskeleton position and velocity, and contact torque are filtered with the same second order low pass filter to calculate the reference stiffness.

In the second experiment section, we use a second order butterworth bandpass filter [33] with cutoff frequency of 1.2 Hz and 10 Hz for exoskeleton position and velocity, and contact torque to filter out the influence of human voluntary movement when calculating the reference stiffness.

For both sections, exoskeleton position and velocity are filtered by the same second order low pass filter as previously mentioned to build the training data set.

2) *Time Domain Regression*: In order to obtain a reference stiffness value for training the online estimation model and validating the accuracy, we use a linear regression for the time domain data regarding the dynamic equation¹

$$m_h \ddot{\theta} + b_h \dot{\theta} + k_h (\theta - \theta_0) = \tau_c \quad (1)$$

where τ_c is the contact torque between the human and exoskeleton, m_h , b_h , and k_h are the inertia, linear damping, and stiffness of the human, θ , $\dot{\theta}$ and $\ddot{\theta}$ are the joint position, velocity and acceleration of the human, and θ_0 is the origin of the human spring. In the case of a rigid connection between the human and exoskeleton, the human's joint position, velocity and acceleration are equal to the corresponding

measurable properties of the exoskeleton. Through a linear regression between τ_c and $[\theta, \dot{\theta}, -1]$ for the corresponding experimental data ($\ddot{\theta}$ is not included due to the amplified noise from the double differentiation on joint position), we find the human stiffness k_h as the reference stiffness, linear damping b_h , and offset spring torque $\tau_0 = k_h \theta_0$. Each linear regression includes 400 pairs of time data samples.

3) *Random Forest Predictor*: We use a random forest predictor from scikit-learn package [35] in Python to estimate muscle stiffness based on a 7-dimensional training data set, which includes the absolute value of exoskeleton position and velocity, filtered by the second order low pass filter, and $S1$, $S2$, $E1$, $E2$ and $E3$. The reference stiffness values are used as a supervisory signal. The model is structured with an estimator number of 50 and a maximum depth of 10 for each estimator to avoid over-fitting. The predictor is trained offline with data from both the first and second experimental sections. The full diagram of the model training procedure is outlined in Fig. 2.

D. Results

We obtain 76350 offline shuffled data points where 50900 are used for offline training and the remaining 25450 are used as an offline test set. The estimation results for all data sets using the trained random forest predictor give us a maximum error of 16.58 Nm/rad and an error variance of 2.55 Nm²/rad². The results are shown in Fig. 3(a). Estimation results for test data set only have a maximum error of 14.51 Nm/rad and an error variance of 3.01 Nm²/rad². Good representatives of validation results are shown in Fig. 3(b) and Fig. 3(c) respectively.

From Fig. 3(a) we notice a significant linear relationship between stiffness estimation and reference stiffness. Comparing the estimation results with other similar research, our R factor 0.993 points to a stronger correlation than the best result of elbow stiffness in [21] of 0.9266 ([21] uses

¹Here, we use a linear damping model to estimate the human's stiffness, because of difficulties implementing hysteretic damping in the time domain regression. Hysteretic damping models are likely more accurate[34], and we use them for the stability analysis.

an artificial neural network to estimate multi-joint stiffness, but we only compare the elbow joint stiffness results). Our stiffness ranges from 5 to more than 90 Nm/rad which is a more reasonable range compared with [21] with a range of 1 to 3 Nm/rad. Our predictor has a maximum error less than 17 Nm/rad while Fig.5 in [22] shows a maximum error greater than 30 Nm/rad and the results in [23] show a maximum error greater than 80 Nm/rad. However, [23] uses a different definition of elbow stiffness and includes data for nine subjects, which may influence their estimation accuracy. In addition, all the experiments in [21], [22], [23], [25] are done without the human's voluntary movement, which weakens the validation of their models. Stiffness estimation in the presence of voluntary motion introduces new challenges, because these voluntary movements can be confused with the human's response to the perturbation. Our bandpass filter helps to remove the influence of human voluntary motion in the estimation procedure (the human's voluntary motion is below the lower cutoff frequency), but does not completely eliminate this influence. This implies that the reference human stiffness is not entirely trustworthy for the second experiment set. However, our compliance shaping controller using a model trained based on this reference stiffness, which we will discuss later, is still stable. This means this error in the training data was compensated by the tuning of the controller's safety bound parameters.

The error between estimated stiffness and reference stiffness may come from three sources: error caused by incorrect sensor data, error caused by the imperfect predictor, and error due to incorrect reference stiffness. The green circle of Fig. 3(b) demonstrates a sudden peak in the stiffness estimate, a peak which is not reflected in the smooth reference stiffness. This kind of instant peak may be caused by inaccurate sensor data corrupting the inputs to the stiffness predictor. An erroneous momentary sensor value may be due to buffer error or electrical noise, which will cause the predictor to return an incorrect estimation result. In Fig. 3(c), the error shown in the orange circle may be a pure inaccuracy from the predictor while the error in the black circle may be caused by the incorrect reference stiffness. Since k_h in Fig 3(c) is acquired using a band pass filter, this unusual sudden increase and decrease of reference stiffness in the black circle can be explained by human motion being abrupt enough to enter the bandpass region of the filter.

In general, our predictor gives an accurate stiffness estimation for both stiffness in isometric conditions and during voluntary movement. This random forest predictor can be used for online stiffness estimation. If we eliminate the data from the stretch sensors in the training data set, we notice a decrease of R factor from 0.993 to 0.987 and an increase of maximum error from 16.58 to 19.32 Nm/rad. The error variance also increases from 2.55 to 5.13 Nm²/rad² validating the importance of including the data from the stretch sensors.

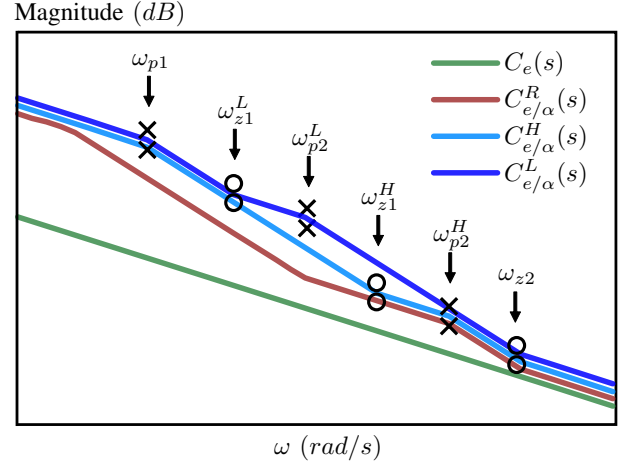


Fig. 4: Conceptual bode plot shows the amplification performance for both the robust controller and the adaptive controller. $C_e(s)$ corresponds to the exoskeleton compliance. $C_{e/α}^H(s)$ and $C_{e/α}^L(s)$ correspond to the human side compliance of the exoskeleton using the adaptive controller when the human has a high stiffness and low stiffness. $C_{e/α}^R(s)$ corresponds to the human side exoskeleton compliance using the robust controller.

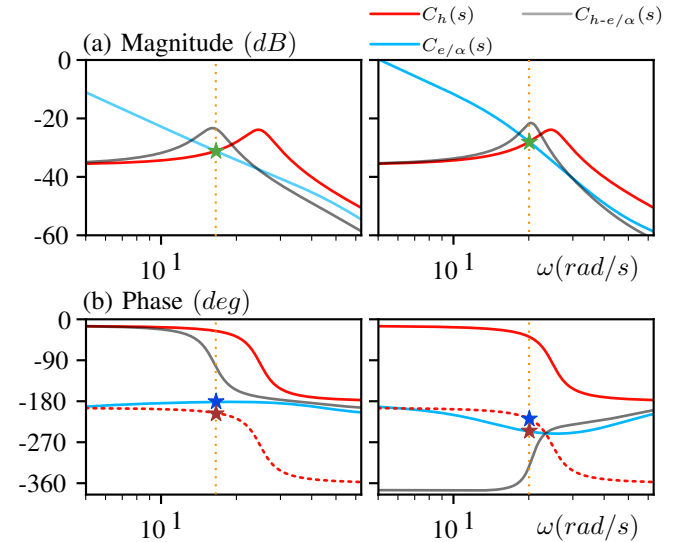


Fig. 5: Bode plot showing stability behaviour. The red dashed line in the phase plot is equal to $\phi(C_h(s)) - 180^\circ$. The phase difference between the blue line and red dashed line determines the stability of the system. The left graph shows a stable system and corresponding phase behavior of the human in exoskeleton with conservative values of λ_1 and λ_2 . The right graph shows an unstable behavior corresponding to more aggressive values of λ_1 and λ_2 .

III. APPLICATION

Since we have demonstrated that stiffness can be estimated online to a reasonable accuracy, we can now exploit this knowledge to design higher performance exoskeleton controllers.

A. Model

We propose a compliance shaping controller, which benefits from the application of online stiffness estimation. The controller aims to achieve a frequency dependent amplification rate expressed as

$$\alpha(s) = \frac{(s^2 + 2\zeta_0\omega_{z1}s + \omega_{z1}^2)(s^2 + 2\zeta_1\omega_{z2}s + \omega_{z2}^2)}{(s^2 + 2\zeta_0\omega_{p1}s + \omega_{p1}^2)(s^2 + 2\zeta_0\omega_{p2}s + \omega_{p2}^2)}, \quad (2)$$

which has its steady state amplification rate $\alpha_{ss} = (\omega_{z1}^2\omega_{z2}^2)/(\omega_{p1}^2\omega_{p2}^2)$. ω_{z2} is 10 Hz based on the bandwidth of the low level force controller. We define two tuning parameters λ_1 and λ_2 as

$$\lambda_1 = \frac{\omega_{h-e}}{\omega_{z1}}, \quad \lambda_2 = \frac{\omega_{p2}}{\omega_{h-e}}, \quad (3)$$

where $\omega_{h-e} = \sqrt{k_h/m_{h-e}}$ is the natural frequency of the human in the exoskeleton and m_{h-e} is the inertia of the human and exoskeleton including the attached weight. The forearm inertia m_h has been measured for an average human at 0.1 kg m² in [11], but we do not know the inertia of our own subject.

In steady state, we have

$$\omega_{z1} = \frac{\omega_{h-e}}{\lambda_1} = \frac{1}{\lambda_1} \sqrt{\frac{k_h}{m_{h-e}}}, \quad (4)$$

$$\omega_{p2} = \lambda_2 \omega_{h-e} = \lambda_2 \sqrt{\frac{k_h}{m_{h-e}}}, \quad (5)$$

$$\omega_{p1} = \frac{\omega_{z1}\omega_{z2}}{\sqrt{\alpha_{ss} \cdot \omega_{p2}}}, \quad (6)$$

where λ_1 , λ_2 and the estimated value of \hat{k}_h determine the values of ω_{z1} , ω_{p1} and ω_{p2} and the shape of our compliance shaping controller. This allows us to increase bandwidth of amplification by changing the shape of our amplification in real time. We refer to this real time compliance shaping controller as an adaptive controller in this paper. In contrast, without real time stiffness estimation, we have to use the most conservative bound of human stiffness to calculate ω_{z1} , ω_{p1} and ω_{p2} , which limits our bandwidth of amplification. We refer to this as the robust controller.

The relationship between exoskeleton position and external torque can be expressed as

$$m_e s^2 \cdot \theta = \tau_e + \tau_c + \tau_s. \quad (7)$$

where τ_e is environment torque, τ_c is torque applied by the human equal to contact torque and τ_s is the amplification torque equal to the actuator torque measured by the P0 exoskeleton encoder. m_e is the inertia of the exoskeleton including the attached weight. We implement the compliance shaping amplification controller as $\tau_s = (\alpha(s) - 1)\tau_c$ so as to achieve the nominal behavior

$$m_e s^2 \cdot \theta = \tau_e + \alpha(s)\tau_c, \quad (8)$$

where the human is amplified by a factor of $\alpha(s)$.

Let us define the compliance of the exoskeleton $C_e(s)$ as

$$C_e(s) = \frac{1}{m_e s^2}. \quad (9)$$

The amplification controller allows the human to feel an

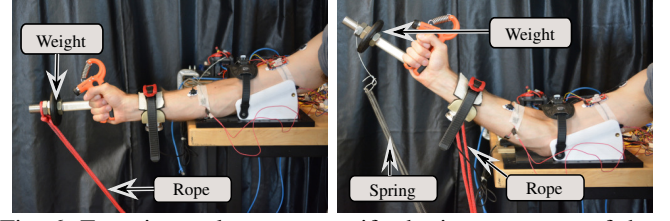


Fig. 6: Experimental setup to verify the improvement of the controller. The left picture shows the setup of the bandwidth test and the right picture shows the setup of the stability test. The rope is in place to maintain a constant position in the bandwidth test and limit the range of position to protect the actuator in the stability test. In both tests, a 1.25 lb weight is attached to the end of the long bar.

attenuated compliance $C_{e/\alpha}(s)$ of the exoskeleton as

$$C_{e/\alpha}(s) = \frac{\alpha(s)}{m_e s^2}. \quad (10)$$

Thus, $C_{e/\alpha}(s)$ reflects the amplification performance of the controller. The conceptual bode plot shown in Fig. 4 illustrates the improved performance using stiffness estimation and shows the amplification performance in different frequencies and values of stiffness. It is straightforward to find a better amplification performance of the compliance shaping controller with online stiffness estimation because the amount of uncertainty handled by the controller is reduced. The difference between the lines corresponding to $C_{e/\alpha}^H$ (the compliance shape when the human stiffness is high) and $C_{e/\alpha}^L$ (the shape when it is low) indicates the controller's shape changing with different stiffness values. In either case the steady state amplification behavior continues until ω_{p1} , a far higher bandwidth than that achieved by $C_{e/\alpha}^R$, the compliance shape that is robust to both human stiffness extremes.

The compliance of the human, $C_h(s)$, is based on the complex stiffness model proposed in [34] as

$$C_h(s) = \frac{1}{m_h s^2 + k_h + c_h j}, \quad (11)$$

where c_h is the hysteretic damping of the human. According to [34],

$$\zeta_h = \frac{c_h}{2k_h}, \quad (12)$$

where ζ_h is the damping ratio of the human's elbow joint determined as a constant value for different subjects [34], [36], [37]. We use a conservative damping ratio of 0.13 for our subject in the simulation.

If we consider a parallel connection between human compliance and human side exoskeleton compliance, we have the compliance of the human in the exoskeleton $C_{h-e/\alpha}(s)$ as a harmonic sum

$$C_{h-e/\alpha}(s) = \left(\frac{1}{C_h(s)} + \frac{1}{C_{e/\alpha}(s)} \right)^{-1}. \quad (13)$$

The stability of our system is determined by the phase margin of $P(s)\alpha(s)$ where $P(s)$ is the plant transfer func-

tion.

$$P(s) = \frac{m_h s^2 + k_h + c_h j}{m_e s^2} \quad (14)$$

$$P(s)\alpha(s) = \frac{\alpha(s)}{m_e s^2} (m_h s^2 + k_h + c_h j) = \frac{C_{e/\alpha}(s)}{C_h(s)}. \quad (15)$$

Therefore, the stability of this system can also be determined by the “human phase margin” of $C_{e/\alpha}(s)$,

$$\Delta\phi = \phi(C_{e/\alpha}(s)) - (\phi(C_h(s)) - 180^\circ). \quad (16)$$

The bode plot in Fig. 5 also introduces the stability behavior of the human in the exoskeleton for different values of λ_1 and λ_2 , which serve as safety buffers for the controller. As their values increase the phase margin of the system increases, but the bandwidth decreases. The margins in Fig. 5.(a) are so large that the amplification behavior is hard to notice in the magnitude plot, as most of it occurs below the plotted frequency range.

As mentioned before, we do not know the inertia of our subject. Fortunately, in (16) reducing the phase of the human compliance increases the phase margin. Inertia causes the human compliance phase to transition from its low frequency behavior to -180° at high frequencies, which is universally a decrease. Thus all human inertia greater than zero increases the phase margin relative to the case where human inertia is zero. We calculate conservative estimates for λ_1 and λ_2 based on the assumption of zero human inertia. In a more realistic test with human inertia based on [11], these parameters are confirmed to be stable.

B. Experiment Validation

We performed three tests to verify the stability, and bandwidth increase of the compliance shaping controller that incorporates the online stiffness estimation, as well as the significance of accurate online stiffness estimation.

1) *Stability Test:* We verify stability of the two controllers using a step response test. The experimental apparatus shown in the right image of Fig. 4 incorporates a spring attached to the end of the exoskeleton to induce an external force on the device. The removal of this spring acts as a step force excitation to the system.

The first experiment tests the robust controller. The participant wears the exoskeleton without the sEMG and stretch sensors and maintains a constant position while the spring is attached. After 10 seconds we remove the spring and observe the step response in the position signal. We repeat this procedure for a low stiffness (no gripper) and high stiffness case (the participant squeezes the gripper of 72 lb).

For the second experiment we repeat the same procedure, but using the adaptive controller. The participant wears the sEMG sensors and stretch sensors to allow a real-time muscle stiffness estimate, which is also observed.

2) *Bandwidth Increase Test:* This experiment is designed to compare the bandwidth of the adaptive controller with the robust controller. The experimental setup shown in the left image of Fig. 4 incorporates a rope attached to the end of the exoskeleton to maintain a constant position by pulling against the hard-stop.

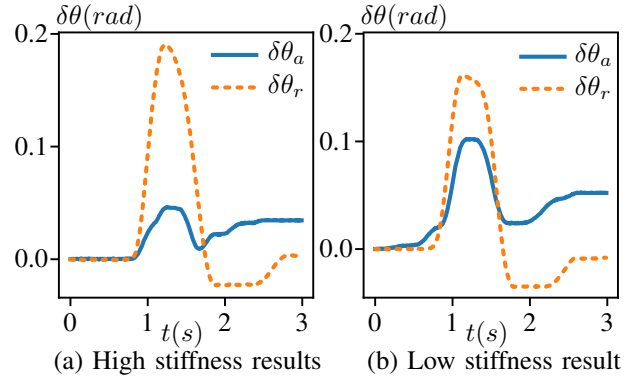


Fig. 7: Stability test response shown by the exoskeleton position changing with time. $\delta\theta_a$ is the position change response of the adaptive controller and $\delta\theta_r$ is the robust controller response.

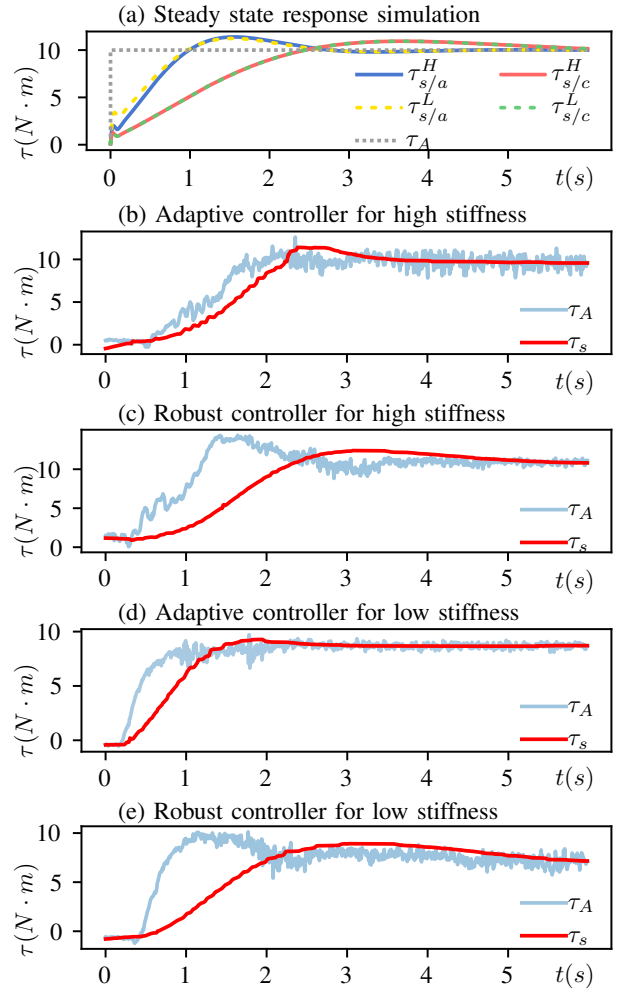


Fig. 8: Steady state response for the bandwidth increase test. τ_s is the actuator torque. τ_A is equal to $-\alpha_{ss}\tau_c$ where τ_c is the contact force between the human and exoskeleton measured by the force sensor around the cuff. τ_A is the amplification torque we want to achieve. $\tau_{s/a}^H$ and $\tau_{s/a}^L$ are the simulated actuator torques of the adaptive controller in high stiffness and low stiffness. $\tau_{s/c}^H$ and $\tau_{s/c}^L$ are the simulated actuator torques of the robust controller in high stiffness and low stiffness.

In order to verify the bandwidth improvement of the adaptive controller, the participant wears the exoskeleton and generates a (near) constant force for 10 seconds. Actuator torque is observed. This process is repeated for the robust controller.

3) *Instability Test*: The significance of accurate online stiffness estimation is measured by using the adaptive controller *without* real stiffness estimate data. Instead, a dummy stiffness estimate (60 Nm/rad) is used. In addition, the participant does not wear sEMG or stretch sensors. The setup is as the stability test, except that the step input is unnecessary. The subject maintains a constant position and relaxes their muscles for 10 seconds while the controller loses stability. After 10 seconds the participant maximally tenses their muscles and the controller regains stability.

C. Results

Results from these experiments are shown in Fig. 7, Fig. 8 and Fig. 9 respectively.

Fig. 7 shows that both controllers give a stable response to an impulse input, however the adaptive controller produces a smaller vibration amplitude than the robust controller for both cases of high stiffness and low stiffness. The lower overshoot amplitude of the adaptive controller response may be due to a better human phase margin and correspondingly better damping ratio in the human-robot system.

Fig. 8 shows both the simulation results of the steady state response with a step input (Fig. 8(a)) as well as experimental results (Fig. 8(b-e)). Fig. 8(b)(c) shows the comparison of the robust controller and the adaptive controller in the high stiffness case and Fig. 8(d)(e) show the low stiffness case. The time difference between τ_s and τ_A indicates the bandwidth of the controller. In both cases, the adaptive controller requires less time to achieve the target torque τ_A and therefore has a higher bandwidth. The experimental results appear consistent with the simulation results—large visual differences in the plots are largely due to the human input deviating from a perfect step.

Fig. 9 shows the instability test result. When the adaptive controller has a discrepancy between estimated stiffness value and the actual stiffness value, the system becomes unstable when the human stiffness is far from the estimated value, as shown in Fig. 9. This experiment highlights the importance of accurate stiffness estimation to our adaptive controller.

IV. DISCUSSION

Many studies performed on amplification exoskeletons have relied on conservative bounds of human impedance properties [7], [13], [34]. Due to the difficulties of online estimation of human muscle stiffness [21], [22], [23], [25], few studies have attempted to improve amplification controller performance using these properties.

In this paper, we propose an adaptive compliance shaping controller and demonstrate the improved performance due to stiffness estimation. The adaptive controller using the stiffness estimation provides increased stability and higher

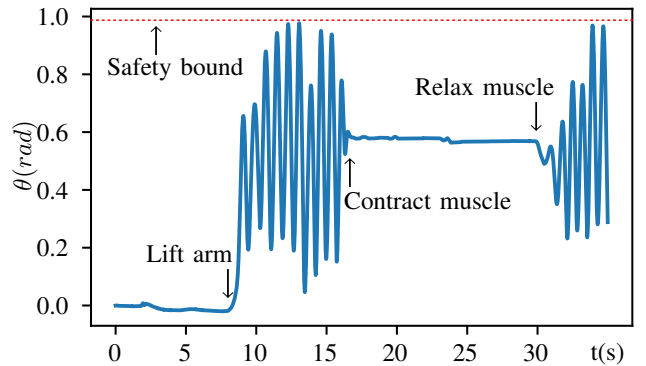


Fig. 9: The instability test. The red dotted line at the top of the graph is the maximum position, as limited by the rope shown in the right picture of Fig. 6.

bandwidth than a comparable robust controller designed based on a conservative bound of human stiffness. We prove this improvement both theoretically and experimentally on a one DOF exoskeleton.

Accurate stiffness estimation is necessary to realize this compliance shaping controller. And our random forest predictor—using data from both sEMG and stretch sensors—was sufficiently accurate. Our two experiment sections include training data from both isometric conditions and dynamic conditions with voluntary movement. Our estimation results appear to be more accurate than similar studies [21], [22]. The estimation results might be further improved with better and more reliable sensors, as well as by taking into consideration the time delay of the filter. A higher accuracy would allow us to use a lower safety bound λ_1 and λ_2 to achieve even higher bandwidth.

The convergence of the random forest predictor has not been proven, so it is hard to make guarantees about the performance and safety of the predictor. As future work, we propose to integrate a backup safety controller [38] to take over if the learning system fails. Such a backup controller could offer firm safety guarantees, but would not interfere with the controller if it was not misbehaving.

The bandwidth increase test and the stability test point to performance improvement that can be realized with information about human properties. In this paper, we use very conservative values of λ_1 and λ_2 , calculated based on a zero human inertia assumption, for both the adaptive and robust controller, which limits the performance of both controllers. In future studies, if we know the accurate value of human inertia we can use a more aggressive safety bound to achieve better performance for both controllers. However, we can still expect the adaptive controller to outperform the robust controller. We believe this method can be applied to other kinds of controllers currently lacking knowledge of human impedance parameters. For instance the controllers in [7], [13], [34] might achieve similar bandwidth improvements if they had a similar system to update the human model online.

REFERENCES

- [1] O. Harib, A. Hereid, A. Agrawal, T. Gurriet, S. Finet, G. Boeris, A. Duburcq, M. E. Mungai, M. Masselin, A. D. Ames, K. Sreenath,

- and J. W. Grizzle, "Feedback control of an exoskeleton for paraplegics: Toward robustly stable, hands-free dynamic walking," *IEEE Control Systems Magazine*, vol. 38, no. 6, pp. 61–87, 2018.
- [2] R. J. Farris, H. A. Quintero, S. A. Murray, K. H. Ha, C. Hartigan, and M. Goldfarb, "A preliminary assessment of legged mobility provided by a lower limb exoskeleton for persons with paraplegia," *IEEE Transactions on neural systems and rehabilitation engineering*, vol. 22, no. 3, pp. 482–490, 2013.
 - [3] H. K. Kwa, J. H. Noorden, M. Missel, T. Craig, J. E. Pratt, and P. D. Neuhaus, "Development of the ihm mobility assist exoskeleton," in *2009 IEEE International Conference on Robotics and Automation*. IEEE, 2009, pp. 2556–2562.
 - [4] B. Huang, Z. Li, X. Wu, A. Ajoudani, A. Bicchi, and J. Liu, "Coordination control of a dual-arm exoskeleton robot using human impedance transfer skills," *IEEE Transactions on Systems, Man, and Cybernetics: Systems*, vol. 49, no. 5, pp. 954–963, 2017.
 - [5] M. Bergamasco, B. Allotta, L. Bosio, L. Ferretti, G. Parrini, G. Prisco, F. Salsedo, and G. Sartini, "An arm exoskeleton system for teleoperation and virtual environments applications," in *Proceedings of the 1994 IEEE International Conference on Robotics and Automation*. IEEE, 1994, pp. 1449–1454.
 - [6] G. C. Thomas, J. M. Coholich, and L. Sentis, "Compliance shaping for control of strength amplification exoskeletons with elastic cuffs," *arXiv preprint arXiv:1903.09673*, 2019.
 - [7] B. He, G. C. Thomas, N. Paine, and L. Sentis, "Modeling and loop shaping of single-joint amplification exoskeleton with contact sensing and series elastic actuation," in *2019 American Control Conference (ACC)*. IEEE, 2019, pp. 4580–4587.
 - [8] S. Lee, J. Kim, L. Baker, A. Long, N. Karavas, N. Menard, I. Galiana, and C. J. Walsh, "Autonomous multi-joint soft exosuit with augmentation-power-based control parameter tuning reduces energy cost of loaded walking," *Journal of Neuroengineering and Rehabilitation*, vol. 15, no. 1, p. 66, 2018.
 - [9] M. Fontana, R. Verthey, S. Marcheschi, F. Salsedo, and M. Bergamasco, "The body extender: A full-body exoskeleton for the transport and handling of heavy loads," *IEEE Robotics & Automation Magazine*, vol. 21, no. 4, pp. 34–44, 2014.
 - [10] J. Zhang, P. Fiers, K. A. Witte, R. W. Jackson, K. L. Poggensee, C. G. Atkeson, and S. H. Collins, "Human-in-the-loop optimization of exoskeleton assistance during walking," *Science*, vol. 356, no. 6344, pp. 1280–1284, 2017.
 - [11] S. C. Cannon and G. I. Zahalak, "The mechanical behavior of active human skeletal muscle in small oscillations," *Journal of Biomechanics*, vol. 15, no. 2, pp. 111–121, 1982.
 - [12] D. J. Bennett, J. M. Hollerbach, Y. Xu, and I. W. Hunter, "Time-varying stiffness of human elbow joint during cyclic voluntary movement," *Experimental Brain Research*, vol. 88, no. 2, pp. 433–442, Feb 1992.
 - [13] S. P. Buerger and N. Hogan, "Complementary stability and loop shaping for improved human robot interaction," *IEEE Transactions on Robotics*, vol. 23, no. 2, pp. 232–244, April 2007.
 - [14] R. J. Adams and B. Hannaford, "Stable haptic interaction with virtual environments," *IEEE Transactions on robotics and Automation*, vol. 15, no. 3, pp. 465–474, 1999.
 - [15] A. Q. Keemink, H. van der Kooij, and A. H. Stienen, "Admittance control for physical humanrobot interaction," *The International Journal of Robotics Research*, vol. 37, no. 11, pp. 1421–1444, 2018.
 - [16] T. Tsumugiwa, R. Yokogawa, and K. Hara, "Variable impedance control based on estimation of human arm stiffness for human-robot cooperative calligraphic task," in *Proceedings 2002 IEEE International Conference on Robotics and Automation (Cat. No. 02CH37292)*, vol. 1. IEEE, 2002, pp. 644–650.
 - [17] S. Chen, B. Yao, Z. Chen, X. Zhu, and S. Zhu, "Adaptive robust cascade force control of 1-dof joint exoskeleton for human performance augmentation," in *ASME 2015 Dynamic Systems and Control Conference*. American Society of Mechanical Engineers Digital Collection, 2016.
 - [18] A. Lecours, B. Mayer-St-Onge, and C. Gosselin, "Variable admittance control of a four-degree-of-freedom intelligent assist device," in *2012 IEEE International Conference on Robotics and Automation*. IEEE, 2012, pp. 3903–3908.
 - [19] N. Karavas, A. Ajoudani, N. Tsagarakis, J. Saglia, A. Bicchi, and D. Caldwell, "Tele-impedance based assistive control for a compliant knee exoskeleton," *Robotics and Autonomous Systems*, vol. 73, pp. 78–90, 2015.
 - [20] F. Mussa-Ivaldi, N. Hogan, and E. Bizzi, "Neural, mechanical, and geometric factors subserving arm posture in humans," *Journal of Neuroscience*, vol. 5, no. 10, pp. 2732–2743, 1985.
 - [21] H. K. Kim, B. Kang, B. Kim, and S. Park, "Estimation of multijoint stiffness using electromyogram and artificial neural network," *IEEE Transactions on Systems, Man, and Cybernetics-Part A: Systems and Humans*, vol. 39, no. 5, pp. 972–980, 2009.
 - [22] F. Mobasser and K. Hashtrudi-Zaad, "A method for online estimation of human arm dynamics," in *2006 International Conference of the IEEE Engineering in Medicine and Biology Society*. IEEE, 2006, pp. 2412–2416.
 - [23] D. Shin, J. Kim, and Y. Koike, "A myokinetic arm model for estimating joint torque and stiffness from emg signals during maintained posture," *Journal of neurophysiology*, vol. 101, no. 1, pp. 387–401, 2009.
 - [24] D. W. Franklin, F. Leung, M. Kawato, and T. E. Milner, "Estimation of multijoint limb stiffness from emg during reaching movements," in *IEEE EMBS Asian-Pacific Conference on Biomedical Engineering*, 2003. IEEE, 2003, pp. 224–225.
 - [25] S. Pfeifer, H. Vallery, M. Hardegger, R. Riener, and E. J. Perreault, "Model-based estimation of knee stiffness," *IEEE Transactions on Biomedical Engineering*, vol. 59, no. 9, pp. 2604–2612, 2012.
 - [26] H. Han and J. Kim, "Active muscle stiffness sensor based on piezoelectric resonance for muscle contraction estimation," *Sensors and Actuators A: Physical*, vol. 194, pp. 212–219, 2013.
 - [27] K. Gui, H. Liu, and D. Zhang, "A practical and adaptive method to achieve emg-based torque estimation for a robotic exoskeleton," *IEEE/ASME Transactions on Mechatronics*, vol. 24, no. 2, pp. 483–494, April 2019.
 - [28] J. Nge, T. Tamei, T. Shibata, M. F. F. Orlando, L. Behera, A. Saxena, and A. Dutta, "Control of an optimal finger exoskeleton based on continuous joint angle estimation from emg signals," in *2013 35th Annual International Conference of the IEEE Engineering in Medicine and Biology Society (EMBC)*, July 2013, pp. 338–341.
 - [29] T. Kawase, H. Kambara, and Y. Koike, "A power assist device based on joint equilibrium point estimation from emg signals," *Journal of Robotics and Mechatronics*, vol. 24, no. 1, pp. 205–218, 2012.
 - [30] Z. Li, B. Wang, F. Sun, C. Yang, Q. Xie, and W. Zhang, "semg-based joint force control for an upper-limb power-assist exoskeleton robot," *IEEE Journal of Biomedical and Health Informatics*, vol. 18, no. 3, pp. 1043–1050, May 2014.
 - [31] C. Cheng, T. Huang, and H. Huang, "Bayesian human intention estimator for exoskeleton system," in *2013 IEEE/ASME International Conference on Advanced Intelligent Mechatronics*, July 2013, pp. 465–470.
 - [32] K. Kiguchi and Y. Hayashi, "An emg-based control for an upper-limb power-assist exoskeleton robot," *IEEE Transactions on Systems, Man, and Cybernetics, Part B (Cybernetics)*, vol. 42, no. 4, pp. 1064–1071, Aug 2012.
 - [33] E. Jones, T. Oliphant, P. Peterson *et al.*, "SciPy: Open source scientific tools for Python," 2001–.
 - [34] B. He, H. Huang, G. C. Thomas, and L. Sentis, "Complex stiffness model of physical human-robot interaction: Implications for performance augmentation exoskeletons," *arXiv preprint arXiv:1903.00704*, 2019.
 - [35] F. Pedregosa, G. Varoquaux, A. Gramfort, V. Michel, B. Thirion, O. Grisel, M. Blondel, P. Prettenhofer, R. Weiss, V. Dubourg, J. Vanderplas, A. Passos, D. Cournapeau, M. Brucher, M. Perrot, and E. Duchesnay, "Scikit-learn: Machine learning in Python," *Journal of Machine Learning Research*, vol. 12, pp. 2825–2830, 2011.
 - [36] T. E. Milner and C. Cloutier, "Damping of the wrist joint during voluntary movement," *Experimental Brain Research*, vol. 122, no. 3, pp. 309–317, Sep 1998.
 - [37] F. Lacquaniti, F. Licata, and J. F. Soechting, "The mechanical behavior of the human forearm in response to transient perturbations," *Biological Cybernetics*, vol. 44, no. 1, pp. 35–46, May 1982.
 - [38] G. C. Thomas, B. He, and L. Sentis, "Safety control synthesis with input limits: a hybrid approach," in *2018 Annual American Control Conference (ACC)*. IEEE, 2018, pp. 792–797.